ACS OMEGA

http://pubs.acs.org/journal/acsodf

Article

A Multilayer Interlaced Ag Nanosheet Film Prepared by an Electrodeposition Method on a PPy@PEDOT:PSS Film: A Strategy to Prepare Sensitive Surface-Enhanced Raman Scattering Substrates

Xueqin Wang, Anjiang Lu, Zhongchen Bai,* and Tianwen Xu

Cite This: *ACS Omega* 2022, 7, 9380−9387

Read Online

ACCESS | Metrics & More | Article Recommendations | Supporting Information

ABSTRACT: A highly sensitive multilayer interlaced silver (Ag) nanosheet (MISN) film was prepared on a PPy@PEDOT:PSS film via an electrodeposition method for surface-enhanced Raman scattering (SERS) applications. After the PPy@PEDOT:PSS film was pretreated with ascorbic acid solution, many sparse Ag nanoparticles (NPs) could be directly reduced on the surface of the PPy@PEDOT:PSS film in $AgNO_3$ solution. Then, the MISN film was directionally grown along the surface of sparse Ag NPs by using an electrochemical galvanostatic method to form a Ag/PPy@PEDOT:PSS film for a SERS substrate. The results indicated that with the increase in electrodeposition time, the density of Ag nanosheets was also increased for boosting the SERS effect. Accordingly, owing to the directional growth of Ag NPs, the increase in the length−width ratio of single Ag nanosheets would further promote the SERS signal of the substrate. Moreover, the maximum enhancement factor of the SERS substrate could reach to 12,478, and the minimum limit of detection of melamine solution was down to 5.42 ng/mL. The SERS sensitivity of the Ag nanosheet film reached 100.65. This method of preparing the SERS substrate provides a novel and robust strategy for the low-cost and high-sensitivity detection in biomedicine, drugs, and food.

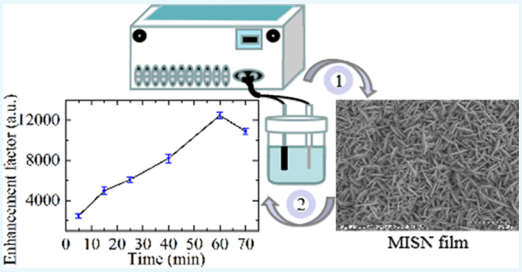

1. INTRODUCTION

Surface-enhanced Raman scattering (SERS), a great enhancement effect of the local electromagnetic field caused by the collective oscillation of electrons in a conductive nanostructure (called the local surface plasmon resonance (LSPR)),[1−3] has been proven to be an ultrasensitive technique to obtain highly specific Raman signals of targeting trace molecules.[4,5] Currently, the SERS technique has been extensively applied in drug analysis,[6] virus detection,[7,8] food safety,[9,10] and biomedical sensors.[11,12] Usually, the efficiency of SERS signals is enormously derived from the geometric shape of metal nanostructures and their gap. Compared with the regular nanostructures (such as spheres), the shape can induce higher-density surface plasmons (SPs). Moreover, the largest enhancement effect has emerged on the overlapped region of differently shaped nanostructures, such as the connection positions of tightly arranged nanostructures or the gap of aggregated nanoparticles (NPs).[1] Therefore, a special morphology and an ultrahigh density are needed to get a suitable enhancement effect of the SERS substrate.

The surfaces of gold (Au), silver (Ag), or copper (Cu) nanostructures can exhibit an effective SERS signal.[13−17] Usually, Ag nanostructures have an excellent physical and chemical property in comparison with other precious metals, which have been widely studied and applied in the fields of optical sensors, biological diagnosis, catalysis, microelectronics, and so on.[18] In addition, owing to the high SERS performance of Ag nanostructures, many meaningful results have been reported in the field of SERS-based biosensors.[19−22] At present, many types of Ag nanostructures have also been synthesized, such as nanorods,[23] NPs,[24,25] nanonets,[26] nanowires,[27,28] nanosheets,[29] etc. Especially, a Ag nanosheet nanostructure has a large surface area for easily adsorbing some biomolecules, which is considered as an ideal material for the SERS detection.

Chemical reduction[30] and light-mediated methods[31] are used for synthesizing the solution-based monodisperse Ag nanosheets, but some liquid Ag nanosheets would result in ineffectivity of SERS applications. Thus, the preparation methods of solid Ag nanosheet films have extensively attracted attention due to the merits of simple processing and low cost. Liu et al.[32] deposited by self-assembly a vertically arranged Ag nanosheet array film by using a polymer-templated electrodeposition method. Mack et al.[33] prepared a continuous Ag nanosheet film on a polyaniline film by using a direct chemical deposition method. In addition, Ma et al.[29] synthesized ultrathin Ag nanosheets through the galvanic replacement

Received: November 12, 2021
Accepted: January 28, 2022
Published: March 8, 2022

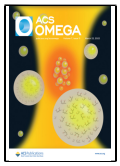

reaction between the $AgNO_3$ and the Cu microcages without any surfactant. Usually, ideal SERS substrates are provided with the characteristics of stability, good economy, well reproducibility, and high sensitivity.[34] Except for the methods mentioned above, other methods also have been used for preparing uniform Ag nanosheets, for instance, nanoimprint lithography, beam etching, template methods, optical lithography, etc. Nevertheless, most of them are not appropriate for multipathway applications due to their harsh experimental conditions, complex preparation procedures, and expensive cost.

A polypyrrole (PPy) film is a kind of conductive polymer, which can be polymerized by the electrodeposition method.[35,36] Furthermore, the PPy film has not only a simple electrodeposition process and low cost but also a uniform conductive surface, well compatibility, and well reducibility. In addition, the PPy film can also uniformly adsorb many functional molecules for fabricating the SERS substrate.[37] Thus, the PPy is also an ideal material for the SERS application.

Herein, we combined a PPy film and a Ag nanosheet film to prepare the Ag/PPy@PEDOT:PSS film for SERS applications by using the electrochemical deposition (ECD) method. The PPy@PEDOT:PSS film was deposited by an electrochemical potentiostatic (ECP) method, and then, ascorbic acid molecules were uniformly adhered on its surface. After the pretreatment with ascorbic acid, the $AgNO_3$ solution was directly reduced to Ag NPs, and then, the SERS substrate of a multilayer interlaced Ag nanosheet (MISN) film was grown via an electrochemical galvanostatic (ECG) method in $AgNO_3$ solution.

2. RESULTS AND DISCUSSION

2.1. Surface Micro-optical Images of the PPy@PEDOT:PSS Film. In Figure 1a,b, the stainless-steel plate had a clear surface morphology, showing that a continuous film was difficult to be prepared by electrodepositing the pyrrole monomer electrolyte. Nevertheless, as shown in Figure 1c, a continuous and homogeneous PPy@PEDOT:PSS film was formed at the same electrodeposition parameters. After adding the PEDOT:PSS, the growth of the polymer film was promoted. The reasons were as follows: (1) The pyrrole monomer covered the PEDOT:PSS surface, and under an electric field, the pyrrole monomer molecules would lose electrons resulting in the surface of the electrode being covered by radical cations. These radical cations could further connect with other pyrrole monomer molecules to polymerize the pyrrole dimer molecules. Like that, the chain of pyrrole molecules was formed. Simultaneously, the PEDOT:PSS molecules were also attached to the surface of the pyrrole molecule chain in the process of pyrrole polymerization to form the PPy@PEDOT:PSS film. (2) The surface of PEDOT:PSS and pyrrole had both negative charges, facilitating the growth of the PPy@PEDOT:PSS film. The PPy@PEDOT:PSS film was grown on the surface of the anode to further confirm these results. In addition, the anions of the PPy@PEDOT:PSS film surface could also adsorb Ag^+ ions to form Ag nanostructures for SERS substrates.

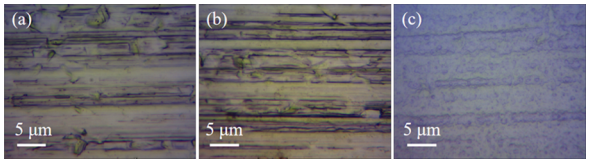

Figure 1. Surface micro-optical images of the stainless-steel plate, the pyrrole film, and the PPy@PEDOT:PSS film. (a) Stainless-steel plate. (b) Pyrrole film. (c) PPy@PEDOT:PSS film.

2.2. Surface Morphologies of the MISN Films. Figure 2 shows SEM images and colors of films with different electrodeposition times. In Figure 2a, the distributions of Ag NPs were uniform, but there was a large number of tiny gaps between Ag NPs, which failed to form a continuous Ag film. Nevertheless, the density and morphology of Ag NPs were changed after this film was electrodeposited in $AgNO_3$-citric acid solution. When the electrodeposition time was increased to 5 and 15 min, their gaps were decreased inch by inch and they had a denser distribution in Figure 2b,c. After electrodeposition for 25 min (Figure 2d), a continuous and gapless Ag film was formed on the PPy@PEDOT:PSS film surface. With a further increased electrodeposition time, the Ag film surface gradually bulged, illustrating that the thickness of the Ag film was also increased. At 60 min, the Ag film became denser and more uniform all over the film surface in Figure 2f. Moreover, the color of the PPy@PEDOT:PSS film would be black. With the growth of Ag NPs and the increase in electrodeposition time, the film color gradually changed from black to yellow. Finally, the Ag nanostructure was grown into the MISN film; correspondingly, its color would be dark yellow.

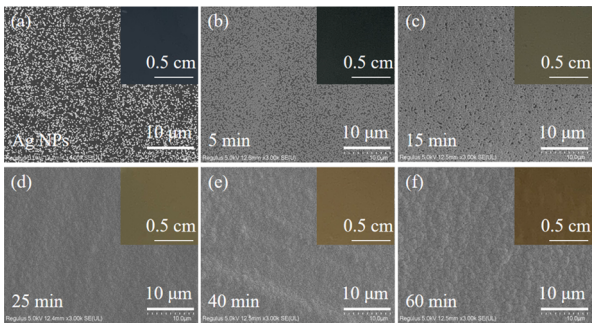

Figure 2. SEM images and colors of films by electrodeposition for (a) 0, (b) 5, (c) 15, (d) 25, (e) 40, and (f) 60 min.

In Figure 3a, the Ag NPs could be considered as Ag nanostructures with irregular grooves, and their sizes were distributed in the range of 160−220 nm and obeyed the Gaussian distribution. This was because after immersion for 24 h, ascorbic acid molecules were fully and uniformly attached to the PPy@PEDOT:PSS film surface. When this film was immersed in $AgNO_3$ solution, Ag NPs would be reduced. The reaction equation was as follows:

$$2Ag^+ + C_6H_8O_6 \rightarrow 2Ag + C_6H_6O_6 + 2H^+ \quad (1)$$

Owing to a short immersion time, the abundant free Ag^+ ions in the $AgNO_3$ solution reacted with the ascorbic acid quickly, and the reduction products were Ag NPs of isotropic nucleation. With the increase in reaction time, more Ag^0 atoms were reduced and self-assembled to form some Ag NP clusters with irregular grooves. Further, Ag NP clusters with different sizes were produced by the different reaction times of Ag^+ ions and ascorbic acid molecules.

https://doi.org/10.1021/acsomega.1c06387
ACS Omega 2022, 7, 9380−9387

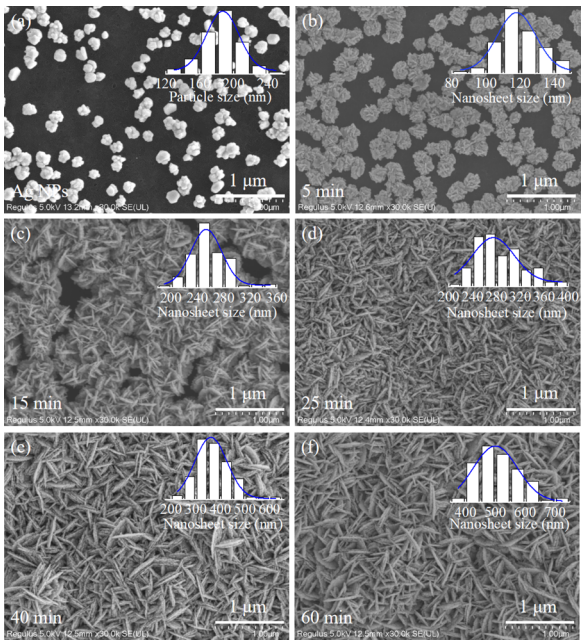

Figure 3. SEM images and the size distribution of Ag nanosheets by electrodeposition for (a) 0, (b) 5, (c) 15, (d) 25, (e) 40, and (f) 60 min.

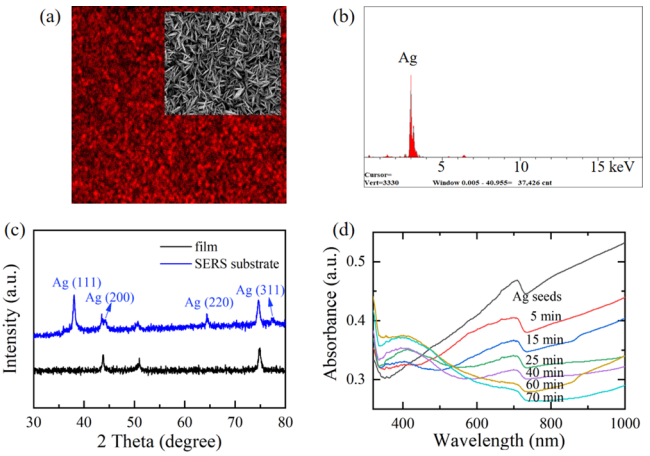

Figure 4. (a) Ag element distribution of the MISN film by electrodeposition for 60 min; (b) EDS result image of (a); (c) X-ray diffraction (XRD) patterns of (a); (d) UV−vis absorption spectra of the Ag/PPy@PEDOT:PSS film by electrodepositing Ag nanostructures for 0, 5, 15, 25, 40, 60, and 70 min.

Moreover, self-assembled Ag NPs acting as Ag seed points were electrodeposited in $AgNO_3$-citric acid mixture solution. There were numerous ridge-like protrusion nanostructures appearing on the surfaces of Ag NP clusters electrodeposited for 5 min in Figure 3b, and the Ag nanosheets were completely formed at 15 min in Figure 3c. In Figure 3d−f, even with increasing the electrodeposition time, the shape of Ag nanosheets no longer changed. Furthermore, the lengths of Ag nanosheets were also enlarged and obeyed Gaussian distribution with the increasing electrodeposition time. With electrodeposition for 60 min, the widths of Ag nanosheets were 400−650 nm. Nevertheless, the shapes of Ag nanosheets were uneven, and the edges were not sharp at 70 min (Figure S1 of the Supporting Information). These results showed that the growth of Ag nanosheets could be regulated by changing the electrodeposition time.

The reasons for the growth of the MISN film were as follows: (1) Owing to the existence of an electric field in the process of electrodeposition, the Ag^+ ions were driven to the surface of the Ag NPs film (the cathode) in the electrolyte to form Ag^0 atoms:

$$Ag^+ + e \rightarrow Ag^0 \quad (2)$$

The grooves in the Ag nanostructures had a lower surface energy to nucleate easily than that of the sharp corners or faceted surfaces,[38,39] so the Ag NP clusters accumulated by the reduced Ag^0 atoms were attached into the grooves. With the increase of reduction of Ag^0 atoms, the Ag nanostructures began to grow isotropically. However, the citric acid molecules acted as a selective stabilizer to promote the growth of the (111) plane and hinder the growth of other planes of Ag NPs.[40] In Figure 4c, the (111) plane of Ag NPs had the strongest diffraction peak, indicating that Ag^0 atoms were preferentially grown in this plane of Ag NPs to form anisotropic Ag nanosheet nanostructures ultimately; (2) With increasing the electrodeposition time, the Ag^0 atoms were also further accumulated, leading to the expansion of the sizes of Ag nanosheets in the vertical direction. Moreover, according to the Ostwald ripening mechanism, the larger surface of Ag NPs had a lower chemical potential energy, so the small Ag NPs migrated to the surface of large Ag NPs for eliminating the gaps between Ag NPs in the horizontal direction to form the first layer of a gapless interlaced Ag nanosheet film; (3) the grooves on the surface of the first layer of the interlaced Ag nanosheet film acted as new nucleation points to grow the second layer of the interlaced Ag nanosheet film. By analogy, the MISN film was generated in the end according to this process. Nevertheless, the uneven shapes and no sharp edges of Ag nanosheets at 70 min were caused by the low concentration of citric acid in the solution owing to the long time of electrodeposition consumption. The morphologies of Ag films without Ag seed points grown before electrodeposition also demonstrated the above formation mechanism of the MISN film (Figure S2 of the Supporting Information).

2.3. Analysis Results of EDS, XRD, Absorption Spectroscopy, and EIS. We measured the EDS and XRD results of the MISN film by electrodepositing Ag nanostructures for 60 min and the UV−vis absorption spectra of the Ag/PPy@PEDOT:PSS film by electrodepositing Ag nanostructures for 0, 5, 15, 25, 40, 60, and 70 min. In Figure 4a, the Ag element had a dense distribution and well uniformity. Figure 4c shows the XRD pattern of the MISN film, the (111), (200), (220), and (311) planes of the Ag face-centered cubic (fcc) structure correspond to four peaks of the Ag crystal at 38.2, 44.3, 64.4, and 77.3°,[41] and the other peaks were from the PPy@PEDOT:PSS film, showing that this MISN film had a well-crystallized Ag nanocrystal. In Figure 4d, with the increasing time of depositing Ag NPs, the absorption peaks of films at 420 nm were increased, indicating that the surface plasma resonance (SPR) effect was also enhanced.[42] When the electrodeposition time was 60 min, the SPR effect reached the strongest. The intensity of the absorption peak at 70 min was weaker than that at 60 min owing to the uneven distribution of nanosheet structures. In Figure S3 of the Supporting Information, the absorption peak of the PPy@PEDOT:PSS film was between 550 and 800 nm, which was overlapped with

https://doi.org/10.1021/acsomega.1c06387
ACS Omega 2022, 7, 9380−9387

that of the Ag nanosheets. Therefore, with the increase in electrodeposition time, the absorption intensities were reduced owing to the thicker thickness of the PPy@PEDOT:PSS film. In addition, the redshift of absorption peaks at 700 nm was obvious due to the increased sizes of nanosheets.[43]

Figure 5 shows the electrochemical impedance spectra (EIS) for preparation processes of MISN films. When the working

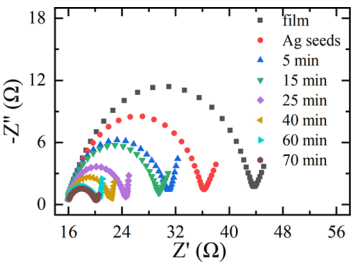

Figure 5. EIS for MISN films.

electrode was the PPy@PEDOT:PSS film, its value of charge transfer resistance (Ret) was the largest, and the Ret was also decreased successively with the growth of Ag NPs and the increase in electrodeposition time. In general, the electron transfer was positively correlated with the Ret on the electrode surface, so the Ret of the MISN film with an extremely high conductivity was merely 4 Ω when electrodepositing for 60 min.

2.4. EFs of SERS Substrates. Figure 6a shows the Raman spectra of melamine powder and the MISN film by electrodeposition for 60 min. There were no obvious Raman peaks in the SERS substrate at 677, 985, and 1561 cm^{-1}, while melamine powder had distinct Raman peaks in these positions. Raman peaks at 677, 985, and 1561 cm^{-1} were respectively derived from the thiotriazinone vibration, the symmetric stretching vibration of −C−NC− bonds, and the bending vibration of −N−H− bonds of melamine molecules.

We selected the strongest Raman characteristic peak of melamine molecules at 677 cm^{-1} to calculate the enhancement factors (EFs). Figure 6b shows the SERS spectra from SERS substrates with different times of electrodepositing Ag nanostructures using 100 μg/mL melamine solutions as a detection sample. In Figure 6c, the relative standard deviation (RSD) values of SERS intensities were calculated from SERS spectra of five different random positions on each substrate. Their RSD values were all less than 10%, indicating that these substrates had good uniformity, stability, and repeatability. The EFs were calculated according to eq 3:[37]

$$\mathrm{EF} = \frac{I_{\mathrm{SERS}} C_{\mathrm{R}}}{I_{\mathrm{R}} C_{\mathrm{SERS}}} \tag{3}$$

Here, the Raman intensities of the sample and the reference sample at 677 cm^{-1} were I_{SERS} and I_R, respectively. Similarly, the melamine solution concentrations of the sample and the reference sample were respectively C_{SERS} and C_R. Table 1 and Figure 6d show the calculated EFs.

Figure 6d shows the relationship between the EFs and the electrodeposition time of SERS substrates. As the increase in electrodeposition time, the EFs of Raman intensities were also gradually increased from 0 to 60 min. However, the EF declined when electrodepositing for 70 min.

The enhanced SERS signals stemmed from multifold effects of the electromagnetic field of the Ag nanostructure surface. (1) Usually, an appropriate incident frequency of a photon illuminated on the surface of Ag nanostructures could induce the SPR effect for boosting Raman signals. For a willow-shaped Ag nanostructure, the SPR effect was complex. In addition to the classical SPR effect, other enhanced effects should be considered. The local electromagnetic field between adjacent metal NPs could enhance the Raman signal. A smaller distance between Ag nanostructures would enhance the electromagnetic field of their gaps, which was called the "hot spot" effect.[44] (2) Furthermore, the strength of SPR highly depended on the shape of nanostructures. For the oblate Ag nanosheet structures, the SPs along the long axis of Ag nanosheets (the

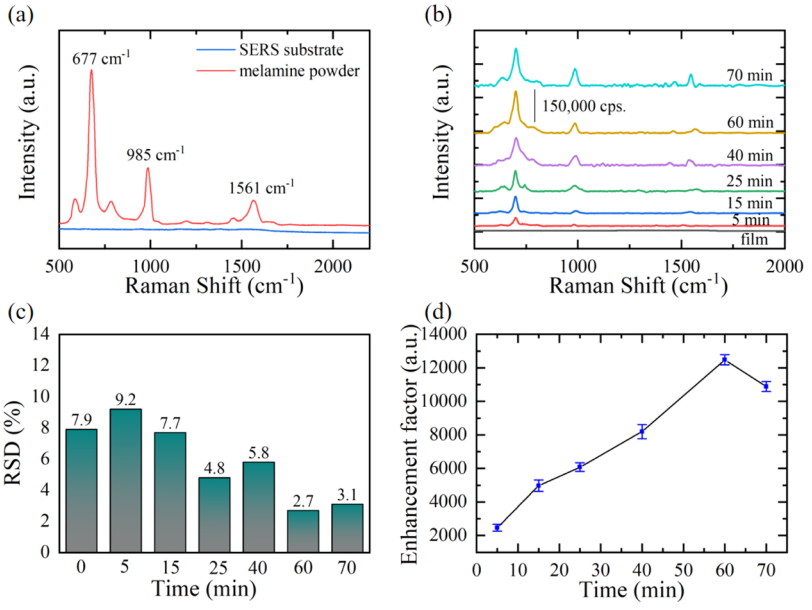

Figure 6. (a) Raman spectra of melamine powder and the MISN film, (b) SERS spectra of Ag nanosheets with different densities, (c) RSD histograms of SERS intensity at 677 cm^{-1}, and (d) relationship between the EFs and the electrodeposition time of SERS substrates.

https://doi.org/10.1021/acsomega.1c06387
ACS Omega 2022, 7, 9380−9387

Table 1. EFs of Raman Intensity under Different Electrodeposition Times

sample	I	II	III	IV	V	VI	VII
electrodeposition time (min)	0	5	15	25	40	60	70
SERS intensity (a.u.)	20	49,259	99,406	121,623	163,971	249,558	217,744
EF		2,463	4,970	6,081	8,199	12,478	10,887

vertical direction of Ag nanosheets) could also result in a narrower SPR compared with the regular Ag NPs. In addition, the edge of Ag nanosheets had a large curvature, which also induced a high electromagnetic field (called the lightning rod effect).[43]

The process of enhancing SERS signals could be explained as follows: (1) The MISNs were excited by a laser with a center wavelength at 633 nm, and the LSPR was generated between adjacent interlaced Ag nanosheets to strengthen the "hot spot" effect horizontally. (2) When the electrodeposition time was longer, a large number of Ag nanosheets accumulated on the film surface resulting in a strong "hot spot" and lightning rod effect; thus, SERS signals were greatly facilitated for boosting the limit of detection from the samples. In Table 1, even if the electrodeposition time was only 5 min, the EF of melamine molecules was as good as 2,463 times, and the Raman signal could be enhanced to 12,478 times when electrodepositing for 60 min. Nevertheless, the Raman signal was reduced at 70 min because the lightning rod effect of Ag nanosheets was weakened owing to the uneven shapes and no sharp edges of Ag nanosheets.

2.5. The SERS Sensitivity and LOD of MISN Films. Here, the MISN film that had the largest EF by electrodeposition for 60 min acted as the SERS substrate to detect the low-concentration melamine molecules. Figure 7a shows the

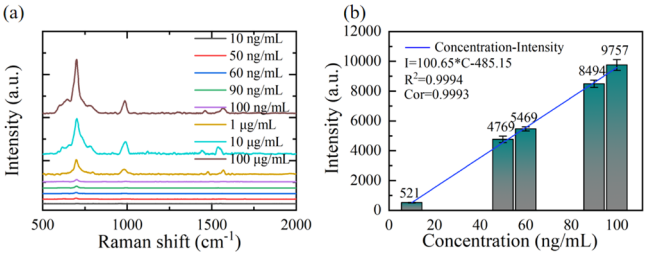

Figure 7. (a) SERS spectra of melamine solutions in different concentrations and (b) linear fitting between the SERS intensity and melamine concentration within the range of 10−100 ng/mL.

SERS spectra of melamine solutions in various concentrations, and the average SERS intensities and standard deviations were calculated from five different random positions under the same melamine concentration in Figure 7b. In Figure 7a, the SERS signal intensity was increased gradually with the increase in melamine concentration, and there was a significant SERS enhanced effect when the melamine solution had a higher concentration. Even if the highest melamine concentration was 100 ng/mL, the intensity of the SERS signal was also significantly enlarged. In addition, when the concentration was 10 ng/mL, the SERS intensity was still 521 units. The linear correlation coefficient and the determination coefficient were respectively 0.9994 and 0.9993 in Figure 7b, showing that an extremely good linear correlation existed between the SERS intensity and melamine concentration within the range of 10−100 ng/mL. Especially, its slope was 100.65 in this range; it illustrated that this film substrate was sensitive to detect the melamine solutions with ultralow concentrations. In addition, the limit of detection (LOD) of melamine solution was 5.42 ng/mL on this SERS substrate, which was obtained in the intersection between the 3× noise level and the equation.

Moreover, 20 and 30 ng/mL melamine solutions had been detected as shown in Figure 8, their SERS signal intensities

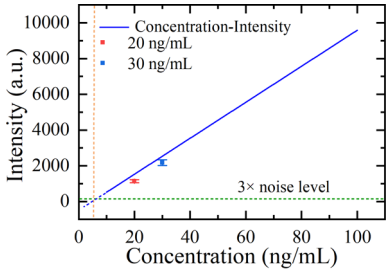

Figure 8. Verification curve of linear relation.

were evenly distributed along this curve, and all recovery rates of 20 and 30 ng/mL melamine solutions ranged from 80 to 100% as shown in Table 2, illustrating that this SERS substrate had well repeatability and reliability.

Table 2. Recovery Rates for the SERS Detection of 20 and 30 ng/mL Melamine Solutions

standard addition concentration (ng/mL)	number	measured SERS intensity (a.u.)	calculated concentration (ng/mL)	recovery rate (%)
20	1	1307	17.8058	89.0290
	2	1126	16.0075	80.0375
	3	1129	16.0373	80.1865
	4	1130	16.0472	80.2360
	5	1139	16.1366	80.6830
	average value	1166.2	16.4069	82.0345
30	1	2275	27.4232	91.4107
	2	2391	28.5758	95.2527
	3	2198	26.6582	88.8607
	4	1949	24.1843	80.6143
	5	2027	24.9593	83.1977
	average value	2168	26.3602	87.8673

3. CONCLUSIONS

We have proposed a simple strategy for preparing a highly sensitive MISN film on the PPy@PEDOT:PSS film via an electrodeposition method for SERS applications. After the PPy@PEDOT:PSS film was pretreated with ascorbic acid solution, Ag NPs were self-assembly reduced on the PPy@PEDOT:PSS film surface in $AgNO_3$ solution. Then, the MISN film was grown by the electrochemical galvanostatic (ECG) method to form a Ag/PPy@PEDOT:PSS structure film for a SERS substrate. The results indicated that the density of Ag nanosheets was increased for boosting its SERS effect due to

https://doi.org/10.1021/acsomega.1c06387
ACS Omega 2022, 7, 9380−9387

the increase in electrodeposition time. With electrodeposition for 60 min, the widths of Ag nanosheets were 400−650 nm. Melamine acted as target detection molecules, and a good SERS activity was observed in this film substrate. In addition, the maximum EF could reach up to 12,478 times, and the minimum LOD of melamine solution could be down to 5.42 ng/mL. In the range of 10−100 ng/mL, an extremely good linear correlation existed between the SERS intensity and melamine concentration. We believe that this kind of MISN film SERS substrate has wide applications in medicine and food; meanwhile, it also provides a novel and well strategy in SERS detection with low cost and high sensitivity.

4. EXPERIMENTAL SECTION

4.1. Experimental Materials. Melamine powder and methanol (AR, Aladdin Reagents Co., Ltd.) acted as a target detection reagent and extracting solution. A stainless-steel plate was used as the cathode for depositing the SERS film, which was purchased from Shanghai Leiyi Electromechanical Equipment Engineering Co., Ltd. Anhydrous ethanol (AR, Aladdin Reagents Co., Ltd.) was used for washing solid samples. The mixture solution of PEDOT:PSS (95%, Merck Reagent Co., Ltd.) and PPy (98%, Merck Reagent Co., Ltd.) was used to deposit the PPy@PEDOT:PSS film on the surface of the stainless-steel plate. Ascorbic acid powder (AR, Merck Reagent Co., Ltd.) and citric acid powder (AR, Merck Reagent Co., Ltd.) acted as the surface stabilizer of Ag nanostructures. $AgNO_3$ powder (AR, Merck Reagent Co., Ltd.) was applied to prepare the Ag NPs and MISN films. $K_3Fe(CN)_6$ powder (AR, Aladdin Reagent Co., Ltd.), $K_4Fe(CN)_6$ powder (AR, Aladdin Reagent Co., Ltd.), and KCl powder (AR, Aladdin Reagent Co., Ltd.) were used for preparing a standard solution for EIS. Before use, all chemical reagents were not further purified.

4.2. Preparation of the MISN Film. Figure 9 shows the preparation processes of the MISN film. Its preparation

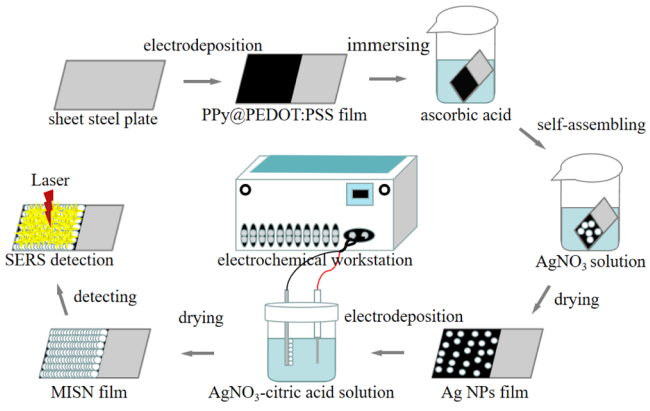

Figure 9. Preparation scheme diagram of the MISN film.

processes involved mainly three steps: (1) electrodepositing the PPy@PEDOT:PSS film, (2) self-assembling Ag NPs on the PPy@PEDOT:PSS film, and (3) electrodepositing the MISN film.

4.2.1. Processes of Electrodepositing PPy@PEDOT:PSS Films. The processes of preparing PPy@PEDOT:PSS films were as follows: (1) 30 mm × 15 mm × 0.02 mm stainless-steel plates were rinsed three times with anhydrous ethanol. Then, they were put into an ultrasonic cleaner to further get rid of surface contaminants. (2) PEDOT:PSS solution (0.7 mL) and 0.7 mL of pyrrole solution were mixed and were then diluted to a 20 mL solution with deionized water to prepare a PPy@PEDOT:PSS electrolyte. (3) The platinum column electrode and the stainless-steel plate acted as the counter electrode (cathode) and the working electrode (anode). A 3 V constant voltage from the electrochemical workstation was loaded on the working electrode for electrodepositing the PPy@PEDOT:PSS film. (4) After electrodeposition for 30 min, the working electrode was removed, and then, it was washed five times with deionized water to clean the unpolymerized electrolyte.

4.2.2. Self-Assembling Ag NPs on the PPy@PEDOT:PSS Films. Ag NPs on the surface of the PPy@PEDOT:PSS film were prepared according to three steps: (1) 0.07 g of ascorbic acid powder and 0.204 g of $AgNO_3$ powder were each dissolved into 20 mL of deionized water to form 20 mL of ascorbic acid solution (0.02 M) and 20 mL of $AgNO_3$ solution (0.06 M). (2) The PPy@PEDOT:PSS film was immersed in the ascorbic acid solution for 24 h to pretreat the film surface, and then, it was washed four times with deionized water to remove the unreacted solution. (3) Again, the pretreated PPy@PEDOT:PSS film was soaked in $AgNO_3$ solution for 38 s to self-assembly grow Ag NPs on the film surface. Then, after taking out and rinsing it with deionized water, it was naturally dried for standby.

4.2.3. Electrodepositing the MISN Films. The MISN film could be synthesized as follows: (1) 0.36 g of citric acid and 0.04 g of $AgNO_3$ powder were dissolved into 20 mL of deionized water to form the $AgNO_3$-citric acid mixture solution. (2) The Ag NPs film of the PPy@PEDOT:PSS substrate was considered as a working electrode (cathode). Moreover, the platinum sheet electrode was used as an anode. A 0.23 mA/cm^2 current was exerted on the electrodes in the ECG method for electrodepositing Ag nanosheets to form the MISN film by Ag growth on the surface of Ag NPs. After electrodeposition for 60 min, the MISN film was taken out and rinsed and then dried for standby.

4.3. Measurement of EIS. $K_3Fe(CN)_6$ powder (0.033 g) and 0.042 g of $K_4Fe(CN)_6$ powder were dissolved in 20 mL of deionized water to prepare a $K_3Fe(CN)_6/K_4Fe(CN)_6$ solution. Then, 0.149 g of KCl powder was added into it to form an impedance electrolyte. To measure the EIS of the MISN film, a Ag/AgCl electrode, a platinum filament, and the sample were respectively used as the reference electrode, the counter electrode, and the working electrode.

4.4. Preparation of Melamine Solutions of Different Concentrations. Melamine powder (10 mg) was dissolved into 100 mL of methanol solution to form the melamine solution. Then, it was diluted to 20 mL solutions with 10,000, 1,000, 100, 90, 60, 50, 30, 20, and 10 ng/mL concentrations. All film samples were soaked in these solutions for 24 h to detect SERS signals.

4.5. Characterization of the MISN Films. The Ag/PPy@PEDOT:PSS film was observed by an optical material microscope (DM-2700, Leica) equipped with a CCD (Andor, 934up) and an optical Raman spectrometer (Andor, SR-500I-B1) equipped with a 633 nm continual excitation laser (Solna, Cobolt 08-NLD). The elemental analyses were performed and surface morphologies of MISN films were measured by an energy-dispersive spectrometer (EDS, Hitachi, SU8100) and a scanning electron microscope (SEM, Hitachi, SU8100). The crystal direction of the MISN film was determined by an X-ray diffractometer (Bruker, D8 Advance).

https://doi.org/10.1021/acsomega.1c06387
ACS Omega 2022, 7, 9380−9387

The absorptions of MISN films were measured by a UV−vis−NIR spectrometer (Shimadzu, UV-2700i). An electrochemical workstation (Vantone, PGSTAT302N) was used for measuring all EIS.

■ ASSOCIATED CONTENT

Supporting Information

The Supporting Information is available free of charge at https://pubs.acs.org/doi/10.1021/acsomega.1c06387.

SEM images and the size distribution of Ag nanosheets by electrodeposition for 70 min (Figure S1), SEM images of the Ag film without Ag seed points growing before electrodeposition (Figure S2), and UV−vis absorption spectrum of the PPy@PEDOT:PSS film (Figure S3) (PDF)

■ AUTHOR INFORMATION

Corresponding Author

Zhongchen Bai − *College of Medicine and Guizhou Province Key Laboratory for Photoelectronic Technology and Application, Guizhou University, Guiyang City 550025, China;* orcid.org/0000-0002-0286-4246; Email: zcbai@gzu.edu.cn

Authors

Xueqin Wang − *College of Medicine and Guizhou Province Key Laboratory for Photoelectronic Technology and Application, Guizhou University, Guiyang City 550025, China;* orcid.org/0000-0002-9590-8788

Anjiang Lu − *Guizhou Province Key Laboratory for Photoelectronic Technology and Application, Guizhou University, Guiyang City 550025, China*

Tianwen Xu − *College of Medicine and Guizhou Province Key Laboratory for Photoelectronic Technology and Application, Guizhou University, Guiyang City 550025, China*

Complete contact information is available at: https://pubs.acs.org/10.1021/acsomega.1c06387

Notes

The authors declare no competing financial interest.

■ ACKNOWLEDGMENTS

This work was supported by the National Natural Science Foundation of China (NSFC) (62065002 and 61865002), the Project of Outstanding Young Scientific and Technological Talents of Guizhou Province (QKEPTRC[2019]5650), the Guizhou Province Science and Technology Platform and Talent Team Project (QKEPTRC[2018]5616), and the Central Government of China Guiding Local Science and Technology Development Plan (QKZYD[2017]4004).

■ REFERENCES

(1) Darienzo, R. E.; Chen, O.; Sullivan, M.; Mironava, T.; Tannenbaum, R. Au NPs for SERS: Temperature-controlled nanoparticle morphologies and their Raman enhancing properties. *Mater. Chem. Phys.* **2020**, *240*, 122143.

(2) Zhu, A.; Ali, S.; Xu, Y.; Ouyang, Q.; Chen, Q. A SERS aptasensor based on AuNPs functionalized PDMS film for selective and sensitive detection of Staphylococcus aureus. *Biosens. Bioelectron.* **2021**, *172*, 112806.

(3) Zoleo, A.; Rossi, C.; Poggi, G.; Rossi, M.; Meneghetti, M.; Baglioni, P. Spotting aged dyes on paper with SERS. *Phys. Chem. Chem. Phys.* **2020**, *22*, 24070−24076.

(4) Lu, S.; Du, J.; Sun, Z.; Jing, C. Hairpin-Structured Magnetic SERS Sensor for Tetracycline Resistance Gene tetA Detection. *Anal. Chem.* **2020**, *92*, 16229−16235.

(5) Wang, C.; Wang, X.; Li, C.; Xu, X.; Ye, W.; Qiu, G.; Wang, D. Silver mirror films deposited on well plates for SERS detection of multi-analytes: Aiming at 96-well technology. *Talanta* **2021**, *222*, 121544.

(6) Hassan, M. M.; Jiao, T.; Ahmad, W.; Yi, X.; Zareef, M.; Ali, S.; Li, H.; Chen, Q. Cellulose paper-based SERS sensor for sensitive detection of 2,4-D residue levels in tea coupled uninformative variable elimination-partial least squares. *Spectrochim. Acta, Part A* **2021**, *248*, 119198.

(7) Sun, Y.; Xu, L.; Zhang, F.; Song, Z.; Hu, Y.; Ji, Y.; Shen, J.; Li, B.; Lu, H.; Yang, H. A promising magnetic SERS immunosensor for sensitive detection of avian influenza virus. *Biosens. Bioelectron.* **2017**, *89*, 906−912.

(8) Yadav, S.; Senapati, S.; Desai, D.; Gahlaut, S.; Kulkarni, S.; Singh, J. P. Portable and sensitive Ag nanorods based SERS platform for rapid HIV-1 detection and tropism determination. *Colloids Surf., B* **2021**, *198*, 111477.

(9) Lin, S.; Li, X.; Fang, G.; Zhao, H.; Wang, L.; Dong, B. Tetragonal Superlattice of Elongated Rhombic Dodecahedra for Sensitive SERS Determination of Pesticide Residues in Fruit. *ACS Appl. Mater. Interfaces* **2020**, *12*, 56350−56360.

(10) Radu, A. I.; Kuellmer, M.; Giese, B.; Huebner, U.; Weber, K.; Cialla-May, D.; Popp, J. Surface-enhanced Raman spectroscopy (SERS) in food analytics: Detection of vitamins B2 and B12 in cereals. *Talanta* **2016**, *160*, 289−297.

(11) Chen, K. H.; Pan, M. J.; Jargalsaikhan, Z.; Ishdorj, T. O.; Tseng, F. G. Development of Surface-Enhanced Raman Scattering (SERS)-Based Surface-Corrugated Nanopillars for Biomolecular Detection of Colorectal Cancer. *Biosensors* **2020**, *10*, 163.

(12) Liu, X.; Yang, S.; Li, Y.; Wang, B.; Guo, J.; Ma, X. Mesoporous Nanostructures Encapsulated with Metallic Nanodots for Smart SERS Sensing. *ACS Appl. Mater. Interfaces* **2021**, *13*, 186−195.

(13) Aziz, S. B.; Abdullah, O. G.; Saber, D. R.; Rasheed, M. A.; Ahmed, H. M. Investigation of Metallic Silver NPs through UV-Vis and Optical Micrograph Techniques. *Int. J. Electrochem. Sci.* **2017**, 363−373.

(14) Cardinal, M. F.; Vander Ende, E.; Hackler, R. A.; McAnally, M. O.; Stair, P. C.; Schatz, G. C.; Van Duyne, R. P. Expanding applications of SERS through versatile nanomaterials engineering. *Chem. Soc. Rev.* **2017**, *46*, 3886−3903.

(15) Yuan, K. S.; Zheng, J. X.; Yang, D. T.; Sanchez, B. J.; Liu, X. J.; Guo, X. J.; Liu, C. S.; Dina, N. E.; Jian, J. Y.; Bao, Z. J.; Hu, Z. W.; Liang, Z. H.; Zhou, H. B.; Jiang, Z. J. Self-Assembly of Au@Ag Nanoparticles on Mussel Shell To Form Large-Scale 3D Supercrystals as Natural SERS Substrates for the Detection of Pathogenic Bacteria. *ACS Omega* **2018**, *3*, 2855−2864.

(16) Polavarapu, L.; La Porta, A.; Novikov, S. M.; Coronado-Puchau, M.; Liz-Marzan, L. M. Pen-on-Paper Approach Toward the Design of Universal Surface Enhanced Raman Scattering Substrates. *Small* **2014**, *10*, 3065−3071.

(17) Polavarapu, L.; Liz-Marzan, L. M. Towards low-cost flexible substrates for nanoplasmonic sensing. *Phys. Chem. Chem. Phys.* **2013**, *15*, 5288−5300.

(18) Xie, W.; Herrmann, C.; Kompe, K.; Haase, M.; Schlucker, S. Synthesis of bifunctional Au/Pt/Au Core/shell nanoraspberries for in situ SERS monitoring of platinum-catalyzed reactions. *J. Am. Chem. Soc.* **2011**, *133*, 19302−19305.

(19) Hao, Z.; Mansuer, M.; Guo, Y.; Zhu, Z.; Wang, X. Ag-NPs on UF-microsphere as an ultrasensitive SERS substrate with unique features for rhodamine 6G detection. *Talanta* **2016**, *146*, 533−539.

(20) Ouyang, L.; Hu, Y.; Zhu, L.; Cheng, G. J.; Irudayaraj, J. A reusable laser wrapped graphene-Ag array based SERS sensor for trace detection of genomic DNA methylation. *Biosens. Bioelectron.* **2017**, *92*, 755−762.

(21) Song, L.; Mao, K.; Zhou, X.; Hu, J. A novel biosensor based on Au@Ag core-shell NPs for SERS detection of arsenic (III). *Talanta* **2016**, *146*, 285−290.
(22) Tzeng, Y.; Lin, B. Y. Silver-Based SERS Pico-Molar Adenine Sensor. *Biosensors* **2020**, *10*, 122.
(23) Ma, L.; Huang, Y.; Hou, M.; Xie, Z.; Zhang, Z. Silver Nanorods Wrapped with Ultrathin Al2O3 Layers Exhibiting Excellent SERS Sensitivity and Outstanding SERS Stability. *Sci. Rep.* **2015**, *5*, 12890.
(24) Saveleva, M.; Prikhozhdenko, E.; Gorin, D.; Skirtach, A. G.; Yashchenok, A.; Parakhonskiy, B. Polycaprolactone-Based, Porous $CaCO_3$ and Ag Nanoparticle Modified Scaffolds as a SERS Platform With Molecule-Specific Adsorption. *Front. Chem.* **2020**, *7*, 888.
(25) Tao, Q.; Li, S.; Ma, C.; Liu, K.; Zhang, Q. Y. A highly sensitive and recyclable SERS substrate based on Ag-nanoparticle-decorated ZnO nanoflowers in ordered arrays. *Dalton Trans.* **2015**, *44*, 3447−3453.
(26) Sharvani, S.; Upadhayaya, K.; Kumari, G.; Narayana, C.; Shivaprasad, S. M. Nano-morphology induced additional surface plasmon resonance enhancement of SERS sensitivity in Ag/GaN nanowall network. *Nanotechnology* **2015**, *26*, 465701.
(27) Jang, S.; Lee, J.; Nam, S.; Ko, H.; Chang, S. T. Large-Area, Highly Sensitive SERS Substrates with Silver Nanowire Thin Films Coated by Microliter-Scale Solution Process. *Nanoscale Res. Lett.* **2017**, *12*, 581.
(28) Xu, D.; Kang, W.; Zhang, S.; Yang, W.; Jiang, H.; Lei, Y.; Chen, J. Fractal theory and controllable preparation of centimeter level silver nanowire arrays and their application in melamine detection as SERS substrates. *Spectrochim Acta A Mol Biomol Spectrosc* **2019**, *221*, 117184.
(29) Ma, B.; Kong, C.; Hu, X.; Liu, K.; Huang, Q.; Lv, J.; Lu, W.; Zhang, X.; Yang, Z.; Yang, S. A sensitive electrochemical non-enzymatic biosensor for the detection of H_2O_2 released from living cells based on ultrathin concave Ag nanosheets. *Biosens. Bioelectron.* **2018**, *106*, 29−36.
(30) Machulek Junior, A.; de Oliveira, H. P.; Gehlen, M. H. Preparation of silver nanoprisms using poly(N-vinyl-2-pyrrolidone) as a colloid-stabilizing agent and the effect of silver NPs on the photophysical properties of cationic dyes. *Photochem. Photobiol. Sci.* **2003**, *2*, 921−925.
(31) Washio, I.; Xiong, Y.; Yin, Y.; Xia, Y. Reduction by the End Groups of Poly(vinyl pyrrolidone): A New and Versatile Route to the Kinetically Controlled Synthesis of Ag Triangular Nanoplates. *Adv. Mater.* **2006**, *18*, 1745−1749.
(32) Liu, S.; Xu, Z.; Sun, T.; Zhao, W.; Wu, X.; Ma, Z.; Zhang, X.; He, J.; Chen, C. Polymer-templated electrodeposition of Ag nanosheets assemblies array as reproducible surface-enhanced Raman scattering substrate. *J. Nanosci. Nanotechnol.* **2014**, *14*, 4608−4614.
(33) Mack, N. H.; Bailey, J. A.; Doorn, S. K.; Chen, C. A.; Gau, H. M.; Xu, P.; Williams, D. J.; Akhadov, E. A.; Wang, H. L. Mechanistic study of silver nanoparticle formation on conducting polymer surfaces. *Langmuir* **2011**, *27*, 4979−4985.
(34) Lin, X. M.; Cui, Y.; Xu, Y. H.; Ren, B.; Tian, Z. Q. Surface-enhanced Raman spectroscopy: substrate-related issues. *Anal. Bioanal. Chem.* **2009**, *394*, 1729−1745.
(35) Akshaya, K. B.; Anitha, V.; Nidhin, M.; Sudhakar, Y. N.; Louis, G. Electrochemical sensing of vitamin B12 deficiency marker methylmalonic acid using PdAu-PPy tailored carbon fiber paper electrode. *Talanta* **2020**, *217*, 121028.
(36) Wang, Y.; Yan, L.; Cheng, R.; Muhtar, M.; Shan, X.; Xiang, Y.; Cui, W. Multifunctional HA/Cu nano-coatings on titanium using PPy coordination and doping via pulse electrochemical polymerization. *Biomater. Sci.* **2018**, *6*, 575−585.
(37) He, Y.; Han, X.; Chen, D.; Kang, L.; Jin, W.; Qiang, R.; Xu, P.; Du, Y. Chemical deposition of Ag nanostructures on polypyrrole films as active SERS substrates. *RSC Adv.* **2014**, *4*, 7202.
(38) Hamilton, D. R.; Seidensticker, R. G. Propagation mechanism of germanium dendrites. *J. Appl. Phys.* **1960**, *31*, 1165−1168.
(39) Avramovic, L.; Ivanovic, E. R.; Maksimovic, V. M.; Pavlovic, M. M.; Vukovic, M.; Stevanovic, J. S.; Nikolic, N. D. Correlation between crystal structure and morphology of potentiostatically electro-deposited silver dendritic nanostructures. *Trans. Nonferrous Met. Soc. China* **2018**, *28*, 1903−1912.
(40) Xue, C.; Metraux, G. S.; Millstone, J. E.; Mirkin, C. A. Mechanistic Study of Photomediated Triangular Silver Nanoprism Growth. *J. Am. Chem. Soc.* **2008**, *130*, 8337−8344.
(41) Liu, G.; Cai, W.; Kong, L.; Duan, G.; Li, Y.; Wang, J.; Cheng, Z. Trace detection of cyanide based on SERS effect of Ag nanoplate-built hollow microsphere arrays. *J. Hazard. Mater.* **2013**, *248-249*, 435−441.
(42) Bhui, D. K.; Bar, H.; Sarkar, P.; Sahoo, G. P.; De, S. P.; Misra, A. Synthesis and UV-vis spectroscopic study of silver nanoparticles in aqueous SDS solution. *J. Mol. Liq.* **2009**, *145*, 33−37.
(43) Kelly, K. L.; Coronado, E.; Zhao, L.; Schatz, G. C. The Optical Properties of Metal NPs: The Influence of Size, Shape, and Dielectric Environment. *J. Phys. Chem. B* **2003**, *107*, 668−677.
(44) Wang, S.; Tay, L. L.; Liu, H. A SERS and electrical sensor from gas-phase generated Ag NPs self-assembled on planar substrates. *Analyst* **2016**, *141*, 1721−1733.

https://doi.org/10.1021/acsomega.1c06387
ACS Omega 2022, 7, 9380−9387